Published in IET Radar, Sonar and Navigation
Received on 8th October 2012
Revised on 31st January 2013
Accepted on 8th February 2013
doi: 10.1049/iet-rsn.2012.0362

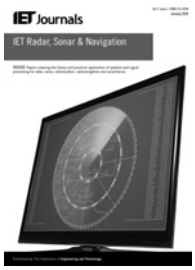

ISSN 1751-8784

Improvement of global navigation satellite system signal acquisition using different grade inertial measurement units for high dynamic applications

Feng Qin[1], *Xingqun Zhan*[1], *Gang Du*[1]

[1]*School of Aeronautics and Astronautics, Shanghai Jiao Tong University, No. 800 Dongchuan Road, Shanghai 200240, People's Republic of China*
E-mail: kevindu@sjtu.edu.cn

Abstract: Most global navigation satellite system (GNSS) receivers cannot work in high dynamic scenarios because of poor navigation satellite acquisition in these environments. Hence, inertial navigation system (INS) is used to aid the GNSS signal acquisition and improve the acquisition capability of the receivers. In INS-aided acquisition, the Doppler estimation accuracy, which has an effect on the acquisition performance, is largely dependent on the quality of the selected inertial measurement unit (IMU). However, the mathematical relation between the IMU errors and the Doppler estimation errors is yet to be determined. This relation is derived and the relation curves are provided. Owing to the insufficiency of the researches on high dynamic applications, such as missiles and aircrafts, a high dynamic scenario is designed and acquisition experiments with different grade IMU assists are performed. The results of these experiments verify that the INS aid can reduce local frequency search space and achieve fast acquisition. Moreover, the experiments also compare the acquisition capabilities of the receivers aided by different grade IMUs and verify the effect of the IMU quality on acquisition performances. Finally, according to these experimental results, a suitable IMU can be determined for the INS-aided acquisition.

1 Introduction

Global navigation satellite system (GNSS) is largely employed to get the position and velocity of various vehicles because of its low cost. However, there is a vital requirement that the GNSS receivers can work only in the scenario where the number of GNSS satellites in view is no less than four. This leads to inconveniences and difficulties for GNSS applications in high dynamic scenarios, where it is not easy to acquire navigation satellites. Hence, the inertial navigation system (INS) carried by most vehicles is used to estimate the position and velocity of high-speed vehicles for eliminating the Doppler frequency shift caused by high dynamics in GNSS signal acquisition. This method is usually called INS-aided acquisition.

In recent decades, GNSS/INS integrated navigation systems have been developed, since the strengths and weaknesses of GNSS receivers and INSs uniquely complement each other. The three well-known architectures of integrated navigation systems are loose coupling, tight coupling and ultra-tight coupling, which are listed in the order of complexity [1–3]. However, these integration schemes pay more attention to navigation and location solutions instead of signal acquisitions. In contrast, the INS-aided acquisition integrates INS and GNSS to improve the acquisition capacity of GNSS receivers before integrated navigation solutions. After the acquisition is aided, a right signal can be provided for every navigation solution in harsh environments.

In the INS-aided acquisition, the Doppler shift of carrier frequency can be estimated by the INS to narrow the uncertainty space and hence achieves faster acquisition. The methodology of the Doppler estimation has been investigated by Progri and Alban [4, 5]. By compensating the estimated Doppler, the receiver's acquisition capability is significantly improved [6, 7]. The INS-aided acquisition can acquire the lower C/N_0 (carrier to noise ratio) signal and can increase the sensitivity of a receiver, which is particularly helpful to detect the presence of the GNSS signal in both dynamic and poor signal environments [8, 9].

Obviously, the INS-aided acquisition has great advantages in the acquisition performance, so it has been investigated for many different applications [9–12]. Previous research work has been focused on low dynamics, such as automotive vehicles, and not on high dynamics. Hence, previous research work has had limited success to prove the acquisition performance improvement induced by the INS aid due to small Doppler shift range caused by vehicle's dynamics. Hence, in this paper, the complicated high dynamic scenario with time-varying large Doppler shift is simulated for high-speed vehicles, such as missiles and aircrafts. In this scenario, a conclusion that the receiver with

the INS aid has better acquisition capacity can be fully verified by the INS-aided acquisition experiments.

In the INS-aided acquisition, the main error sources are the local receiver oscillator and the selected IMU whose quality affects the remaining ambiguities of the frequency shift, which define the size of the acquisition uncertainty space. Some investigations show that the IMU accuracy has a crucial effect on the Doppler estimation errors that determine the INS-aided acquisition performance [13]. However, the mathematical relation between the IMU errors and the Doppler estimation errors, which is yet to be determined, is derived and the relation curves are provided. Furthermore, the relations of the IMU accuracy, the Doppler estimation errors and the INS-aided acquisition performance are proved by the acquisition experiments with different grade IMU assists. Finally, the acquisition capabilities of the receivers aided by different grade IMUs are comprehensively analysed and compared.

2 INS-aided acquisition methodology

The GNSS signal acquisition process consists of a two-dimensional search of the local signal replica in code phase and frequency. The search range of the frequency is the potential maximum frequency shift from the ideal carrier centre frequency, whereas the search range of the code phase is from 0 to 1023 chips. If the correlation result of the local signal and the received signal exceeds the acquisition threshold, the GNSS signal is present in the incoming signal. The correlation output is described as follows [14]

$$s = ADR(\Delta\tau)sinc\left(\pi\Delta f T_{\text{coh}}\right)e\left(j\left(\pi\Delta f T_{\text{coh}} + \Delta\varphi\right)\right) + n \quad (1)$$

where A is the signal amplitude; D is the navigation data; $R(\Delta\tau)$ is the C/A code autocorrelation function; $\Delta\tau$ is the code phase error; Δf is the frequency difference between the received and local signals; $\Delta\varphi$ is the carrier phase error; T_{coh} is the coherent integration time; and n is the white noise.

In (1), the GNSS signal is easier to be acquired, when the Δf is smaller. The T_{coh} is assumed as 1 ms.

In a GNSS receiver, the frequency of a received signal is usually away from the centre frequency due to Doppler shift and oscillator errors. Hence, during the signal acquisition, a wide range of frequency search is inevitable for detecting the presence of a GNSS signal. The larger the Doppler shift, the wider is the search range. It will waste a lot of acquisition time, especially in high dynamic applications. To solve this problem, an INS is used to estimate and remove the Doppler shift to mitigate the frequency ambiguity. Meanwhile, a reduction in the Δf, induced by removing the Doppler shift, can increase the acquisition probability of a GNSS signal.

In the INS-aided acquisition, the Doppler shift is calculated by the position and velocity, which are derived from the INS and the GNSS ephemeris. The parallel code phase search of the software receiver [15, 16] is selected as the search algorithm in the INS-aided acquisition. The predicted Doppler is removed from the searching frequency. Fig. 1 depicts the structure and methodology of this INS-aided acquisition.

3 Frequency shift estimation theory

The frequency shift of a received GNSS signal is mainly caused by the motion of the receiver relative to the satellite and the clock errors in the satellite and receiver. The expression of the main frequency shift is shown as follows [5]

$$f_{\text{shift}} = f_{\text{dyn}} + f_{\text{r,cl}} - f_{\text{s,cl}} \quad (2)$$

where f_{dyn} is the Doppler shift caused by the relative motion between the satellite and the receiver. $f_{\text{r, cl}}$ is the clock error of the receiver, induced by the oscillator error. $f_{\text{s, cl}}$ is the clock error of the satellite, induced by the oscillator error.

Since the atomic clock with high accuracy and stability is selected as the clock of the satellite, the clock error of the satellite $f_{\text{s, cl}}$ can be neglected in the frequency shift estimation.

The Doppler shift f_{dyn} caused by the relative motion between the satellite and the receiver can be calculated from their position and velocity. The equation of the Doppler shift contributed by the receiver and satellite dynamics can

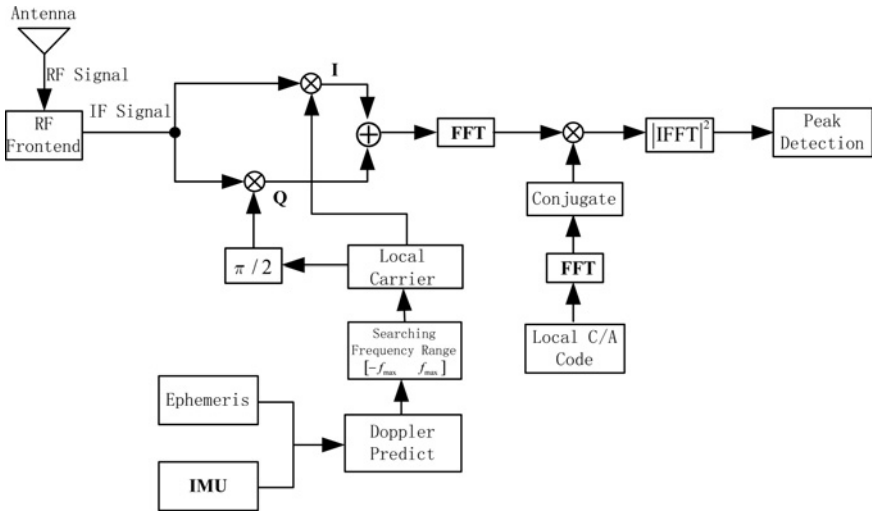

Fig. 1 *INS-aided signal acquisition scheme*

doi: 10.1049/iet-rsn.2012.0362

be written as follows [5]

$$f_{\text{dyn}} = \frac{\bar{V}^{\text{LOS}}}{\lambda_{\text{carr}}} = \frac{\bar{e}_i \cdot \left(\bar{V}^e_{\text{rec}} - \bar{V}^e_{\text{s}}\right)}{\lambda_{\text{carr}}} = f_{\text{r,dyn}} - f_{\text{s,dyn}} \quad (3)$$

where λ_{carr} is the carrier wavelength. $\bar{e}_i$ is the unit vector of the light of sight (LOS), expressed in the Earth-centred, Earth-fixed (ECEF) coordinate frame. $\bar{V}^{\text{LOS}}$ is the light-of-sight (LOS) velocity. $\bar{V}^e_{\text{rec}}$ is the velocity of the receiver and $\bar{V}^e_{\text{s}}$ is the velocity of the satellite, expressed in the ECEF frame, respectively.

The $(1/\lambda_{\text{carr}})$ is only 5.255 and 4.0948 m^{-1} in GPS. Therefore the Doppler shift caused by vehicle's dynamics is largely determined from the inner product $\bar{e}_i \cdot \left(\bar{V}^e_{\text{rec}} - \bar{V}^e_{\text{s}}\right)$ [4, 17]. Typically, a GNSS satellite velocity is approximately 3870.4 m/s. Hence, the maximum relative velocity causes about 5 kHz Doppler shift, for a stationary receiver and a satellite at the horizon [16]. On the other hand, since the receiver velocity is usually less than the satellite velocity, the maximum Doppler shift caused by the receiver dynamics is also 5 kHz.

In (3), the computation of the satellite position and velocity from ephemeris or almanac data are a well-known procedure, described in [18, 19], whereas the inertial navigation computation described in [20] is used to obtain the position and velocity of the receiver from IMU data. Therefore the quality of the selected IMU would affect the accuracy of the Doppler shift estimation.

The clock error of every receiver is different. The error can be estimated based on the navigation solution. The purpose of this paper is to assess the improvement of acquisition capability caused by the INS aid. Hence, some acquisition experiments with large search space are first implemented to calculate the clock error by (4) and compensate the error before the acquisition capabilities of the INS-aided and unaided receivers are compared. Combining the (2) and (3), the expression of the frequency shift is given in (4).

$$f_{\text{shift}} = \frac{\bar{e}_i \cdot \left(\bar{V}^e_{\text{rec}} - \bar{V}^e_{\text{s}}\right)}{\lambda_{\text{carr}}} + f_{\text{r,cl}} \quad (4)$$

The receiver clock error $f_{\text{r, cl}}$ can be calculated from the ephemeris and actual frequency shift measured by the receiver, when the vehicle velocity is set. After several experiments, the error can be estimated with an acceptable accuracy.

4 Doppler shift estimation error

As shown in (3), the Doppler shift is estimated by the LOS velocity, which is calculated from the receiver's position and velocity. Hence, the accuracy of the receiver's position and velocity has a significant effect on the Doppler shift estimation accuracy. Considering that the position and velocity obtained from the INS are not free of errors, the relationship between the position and velocity errors and the LOS velocity error should be built to analyse the Doppler shift estimation error. From the investigation in [21], the relationship has been given as follows

$$\delta f_{\text{dyn}} = \frac{\boldsymbol{\delta}\bar{v}^{\text{LOS}}_i}{\lambda_{\text{carr}}} \quad (5)$$

$$\begin{aligned}\boldsymbol{\delta}\bar{v}^{\text{LOS}}_i = &\left[-\left(\cos L\bar{v}^n + \sin L\bar{v}^u\right)\cos\lambda\bar{e}^x_i - \left(\cos L\bar{v}^n + \sin L\bar{v}^u\right)\right.\\ &\times \sin\lambda\bar{e}^y_i + \left(-\sin L\bar{v}^n + \cos L\bar{v}^u\right)\bar{e}^z_i\left.\right]\delta L\\ &+ \left[\left(-\cos\lambda\bar{v}^e + \sin L\sin\lambda\bar{v}^n - \cos L\sin\lambda\bar{v}^u\right)\bar{e}^x_i\right.\\ &+ \left(-\sin\lambda\bar{v}^e - \sin L\cos\lambda\bar{v}^n + \cos L\cos\lambda\bar{v}^u\right)\bar{e}^y_i\left.\right]\delta\lambda\\ &+ \left(-\sin\lambda\bar{e}^x_i + \cos\lambda\bar{e}^y_i\right)\boldsymbol{\delta}\bar{v}^e\\ &+ \left(-\sin L\cos\lambda\bar{e}^x_i - \sin L\sin\lambda\bar{e}^y_i + \cos L\bar{e}^z_i\right)\boldsymbol{\delta}\bar{v}^n\\ &+ \left(\cos L\cos\lambda\bar{e}^x_i + \cos L\sin\lambda\bar{e}^y_i + \sin L\bar{e}^z_i\right)\boldsymbol{\delta}\bar{v}^u\end{aligned} \quad (6)$$

where δf_{dyn} is the Doppler shift estimation error. $[\bar{v}^e, \bar{v}^n, \bar{v}^u]^{\text{T}}$ is the receiver velocity vector in the local-level (East-North-Up) frame. $[\boldsymbol{\delta}\bar{v}^e, \boldsymbol{\delta}\bar{v}^n, \boldsymbol{\delta}\bar{v}^u]^{\text{T}}$ is the vector of the receiver velocity error in the local-level frame. $[\lambda, L, h]^{\text{T}}$ is the receiver position described as longitude, latitude and height. $[\delta\lambda, \delta L, \delta h]^{\text{T}}$ is the receiver position error. $\boldsymbol{\delta}\bar{v}^{\text{LOS}}_i$ is the vector of the equivalent receiver LOS velocity error for ith visible satellite. $\left[\bar{e}^x_i, \bar{e}^y_i, \bar{e}^z_i\right]^{\text{T}}$ is the unit vector of the LOS for ith visible satellite, expressed in the ECEF frame.

In an INS, the position and velocity errors are mainly caused by IMU biases and drifts, and accumulate over time. Hence, the quality of the IMU selected would determine the position and velocity accuracy of the INS computation, and further affect the Doppler estimation accuracy. To analyse these relations, the models of the INS errors are first built and expressed in the following equations [22]

$$\delta\dot{L} = \frac{\boldsymbol{\delta}\bar{v}^n}{R_M + h} - \delta h\frac{\bar{v}^n}{\left(R_M + h\right)^2} \quad (7)$$

$$\begin{aligned}\delta\dot{\lambda} = &\frac{\boldsymbol{\delta}\bar{v}^e}{R_N + h}\sec L + \delta L\frac{\bar{v}^e}{R_N + h}\tan L\sec L\\ &- \delta h\frac{\bar{v}^e\sec L}{\left(R_N + h\right)^2}\end{aligned} \quad (8)$$

$$\delta\dot{h} = \boldsymbol{\delta}\bar{v}^u \quad (9)$$

$$\begin{aligned}\boldsymbol{\delta}\dot{\bar{V}}^l = &-\boldsymbol{F}^l\bar{\boldsymbol{\varepsilon}}^l - \left(2\boldsymbol{\Omega}^l_{ie} + \boldsymbol{\Omega}^l_{el}\right)\boldsymbol{\delta}\bar{V}^l\\ &+ \bar{V}^l\left(2\boldsymbol{\delta\omega}^l_{ie} + \boldsymbol{\delta\omega}^l_{el}\right) + \boldsymbol{C}^l_b\bar{\boldsymbol{b}}^b + \boldsymbol{C}^l_b\boldsymbol{S}\cdot\bar{\boldsymbol{f}}^b\end{aligned} \quad (10)$$

where R_M is Earth's meridian radius of curvature. R_N is Earth's prime vertical radius of curvature. $\boldsymbol{\delta}\bar{V}^l = [\boldsymbol{\delta}\bar{v}^e, \boldsymbol{\delta}\bar{v}^n, \boldsymbol{\delta}\bar{v}^u]^{\text{T}}$ is the vectors of the receiver velocity error in the local-level frame. $\bar{\boldsymbol{f}}^b$ is the accelerometer measured specific force vector in the IMU body frame. $\boldsymbol{F}^l$ is a skew-symmetric matrix containing the components of the specific force vector $\bar{\boldsymbol{f}}^l$. $\bar{\boldsymbol{\varepsilon}}^l$ is the vector containing the misalignment angle errors of the body frame with respect to the local-level frame. $\boldsymbol{\Omega}^l_{ie}$ is a skew-symmetric matrix of Earth rotation angular rate. $\boldsymbol{\Omega}^l_{el}$ is a skew-symmetric matrix of vehicle transportation angular rate. $\bar{V}^l = [\bar{v}^e, \bar{v}^n, \bar{v}^u]^{\text{T}}$ is the receiver velocity vector in the local-level frame. $\boldsymbol{\delta\omega}^l_{ie}$ is the error in the Earth angular rate. $\boldsymbol{\delta\omega}^l_{el}$ is the error in the vehicle angular rate. $\boldsymbol{C}^l_b$ is the rotation matrix from the body frame to the local-level frame. $\bar{\boldsymbol{b}}^b$ is the vector of accelerometer residual biases in the body frame.

To express the relation between the position and velocity errors and the quality of the accelerometer, (7)–(10) are discretised and accumulated over time. The results are

further given as follows

$$\delta L(k) = \delta L(0) + \sum_{i=0}^{k-1} \left(\frac{\delta \bar{v}^n(i)}{R_M + h(i)} - \delta h(i) \frac{\bar{v}^n(i)}{\left(R_M + h(i)\right)^2} \right) \cdot \Delta t \quad (11)$$

$$\delta \lambda(k) = \delta \lambda(0) + \sum_{i=0}^{k-1} \left(\frac{\delta \bar{v}^e}{R_N + h(i)} \sec L(i) + \delta L(i) \frac{\bar{v}^e(i)}{R_N + h(i)} \tan L(i) \sec L(i) - \delta h(i) \frac{\bar{v}^e(i) \sec L(i)}{\left(R_N + h(i)\right)^2} \right) \cdot \Delta t \quad (12)$$

$$\delta h(k) = \delta h(0) + \sum_{i=0}^{k-1} \delta \bar{v}^u(i) \cdot \Delta t \quad (13)$$

$$\begin{aligned} \delta \bar{V}^l(k) = \delta \bar{V}^l(0) + \sum_{i=0}^{k-1} (& - \boldsymbol{F}^l(i) \bar{\varepsilon}^l(i) \\ & - \left(2\boldsymbol{\Omega}_{ie}^l(i) + \boldsymbol{\Omega}_{el}^l(i)\right) \delta \bar{V}^l(i) \\ & + \bar{V}^l(i) \left(2\delta \boldsymbol{\omega}_{ie}^l(i) + \delta \boldsymbol{\omega}_{el}^l(i)\right) + \boldsymbol{C}_b^l(i) \bar{b}^b \\ & + \boldsymbol{C}_b^l(i) \boldsymbol{S} \cdot \bar{f}^b(i)) \cdot \Delta t \end{aligned} \quad (14)$$

where k represents the kth sampling point. Δt represents the sampling interval.

In (11)–(14), the initial errors of the navigation parameters ($\delta L(0)$, $\delta \lambda(0)$, $\delta h(0)$, $\delta \bar{V}^l(0)$) are assumed to be null. The sampling interval, which is 0.02 s, is usually very small and decided by the IMU sampling rate. The accelerometer residual bias $\bar{b}^b$ consists of constant bias, walking bias and noise, but the constant bias has more effect on the accelerometer bias. After omitting the walking bias and noise, the relationship between the position and velocity errors and the accelerometer constant bias can be derived from (11) to (14). Combining (5), (6) and (11)–(14), the connection between the Doppler estimation error and the constant bias of the selected IMU is built. It is very useful to analyse the effect of the IMU quality on the Doppler estimation accuracy. On the other hand, the inaccurate Doppler estimations would cause the degradation of the GNSS signal acquisition performance, so the quality of the IMU selected is very important in the INS-aided acquisition.

According to the analysis aforementioned, the curves of the relation between the accelerometer constant bias and the Doppler estimation errors of PRN 2 and PRN 9 are depicted in Fig. 2. These Doppler estimation errors are generated by the cumulative error of the INS at the point of 180 s. The errors increase as the accelerometer constant bias increases. The Doppler estimation accuracy decreases rapidly when the constant bias is more than 1 mg. Since the relative motion of the receiver to each satellite is different, the Doppler estimation error for each satellite is different, too.

5 Experiments of the INS-aided acquisition with different IMUs

5.1 Design of simulation scenario

To prove the acquisition performance improvement induced by the INS assist in high-dynamic applications, a simulation scenario is designed for high-speed vehicles, such as missiles and aircrafts. The scenario listed in Table 1 includes the velocity and attitude changes. The initial position is [120°, 30°, 10 000 m] in the Geodetic frame, whereas the initial velocity is [0, 250, 0 m/s] in the body frame. In the scenario, the velocity, acceleration and angular rate are all in the body frame, whereas the attitude is the angle between the body frame and the local-level frame. According to the designed scenario, the movement trajectory of the high-speed vehicle is depicted in Fig. 3.

5.2 IMU data generator

In the INS-aided acquisition, an IMU is used to estimate the vehicle position and velocity for removing the Doppler shift. The IMU data used for the INS computation are generated by a sample mathematical simulation model. The gyro and accelerometer outputs are modelled as follows [23].

In the IMU data generator, the true vehicle rotation rate and acceleration are derived from the movement trajectory [24]. Then, the IMU errors including biases, drifts and noises are added into the true value to simulate the IMU outputs. The performances of the gyro and accelerometer are reflected in the constant bias, walking bias and white noise, which are usually calculated from the constant bias, bias stability and random walk of the gyro and accelerometer [24].

In the INS-aided acquisition, the quality of IMU would affect the acquisition results. Hence, a variety of IMUs are simulated to analyse the acquisition performance changes. By the comparison of the acquisitions with different grade IMUs, the sensor selection in high-dynamic application is

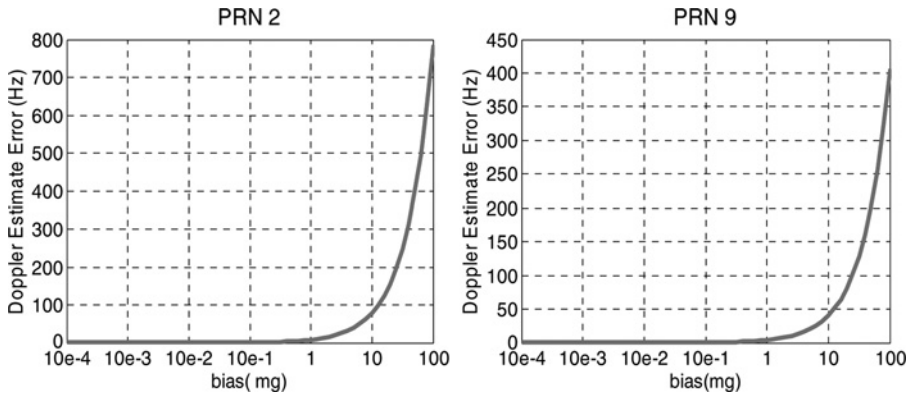

Fig. 2 *Relation between the accelerometer constant bias and the Doppler estimation error of PRN2 and PRN9*

doi: 10.1049/iet-rsn.2012.0362

Table 1 Simulation scenario for high-dynamic applications

Parameter		Section 1	Section 2	Section 3	Section 4	Section 5
time, s		0–7.7	7.7–80	80–110	110–150	150–180
initial velocity, m/s	*x*-axis	0	0	0	0	0
	y-axis	250	1020	1020	1020	1020
	z-axis	0	0	0	0	0
acceleration, m/s^2	*x*-axis	0	0	0	0	0
	y-axis	100	0	0	0	0
	z-axis	0	0	0	0	0
initial attitude, °	pitch angle	0	0	0	0	1.5
	roll angle	0	0	0	0	0
	yaw angle	0	0	0	45	45
angular rate, °/s	*x*-axis	0	0	0	0	0
	y-axis	0	0	0	0	0
	z-axis	0	0	1.5	0	0

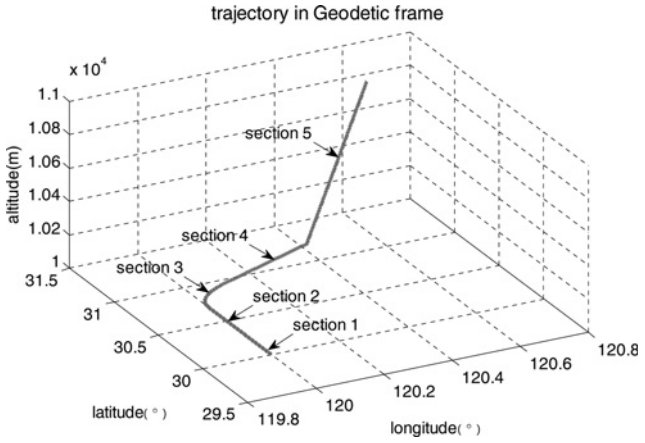

Fig. 3 *Movement trajectory of the high-speed vehicle in the Geodetic frame*

analysed. The parameters of the selected IMUs in the experiments are listed in Table 2 according to [25, 26]. These IMUs are comparable with the products mentioned in [25]. The civil grade IMUs can be used for industry, such as mining and transport, while the tactical grade IMUs can be used for weapon guidance system [27].

5.3 INS computation and Doppler estimation

To estimate the Doppler shift, the vehicle position and velocity have to be computed from IMU data. Furthermore, the position and velocity errors induced by the sensor errors would affect the accuracy of the Doppler estimation. Hence, it is very important to select a suitable IMU for the Doppler estimation and the INS-aided acquisition. The navigation errors of the INSs with the aforementioned four IMUs are illustrated in Figs. 4–7, while the maximum errors in 180 s are further listed in Table 3. The algorithm proposed by Savage [20] is used for the INS computation to get the vehicle position and velocity.

Table 2 IMU parameter in the experiments

IMU parameter		MEMS1	MEMS2	Civil grade	Tactical grade
gyro errors	constant bias, °/*h*	300	20	1	0.01
	bias stability, °/*h*	300	20	0.1	0.001
	random walk, [$^\circ/\sqrt{h}$]	30	0.4	0.001	0.0005
accelerometer errors	constant bias, *mg*	10	1	0.1	0.01
	bias stability, *mg*	10	0.5	0.01	0.001
	random walk, [$m/s/\sqrt{h}$]	1	0.01	0.005	0.0005

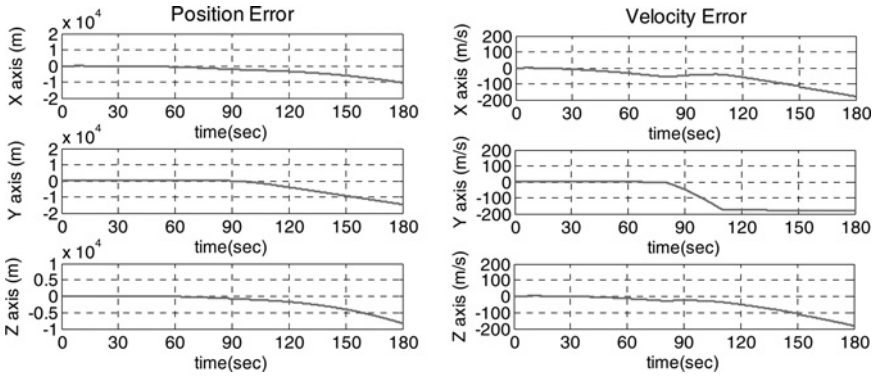

Fig. 4 *Position and velocity errors of INS with the MEMS IMU1*

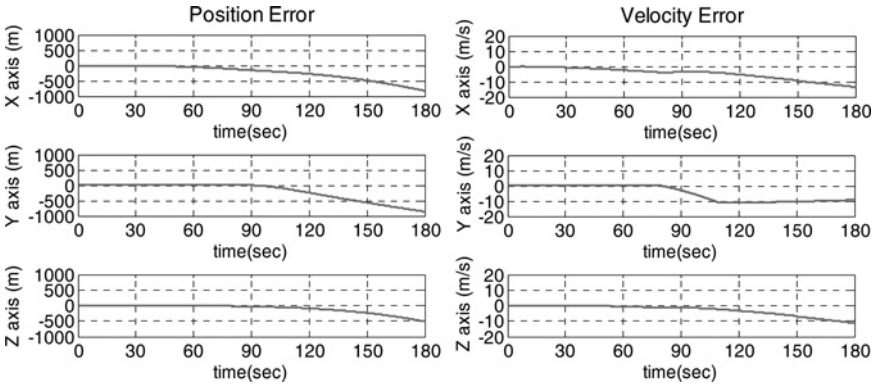

Fig. 5 *Position and velocity errors of INS with the MEMS IMU2*

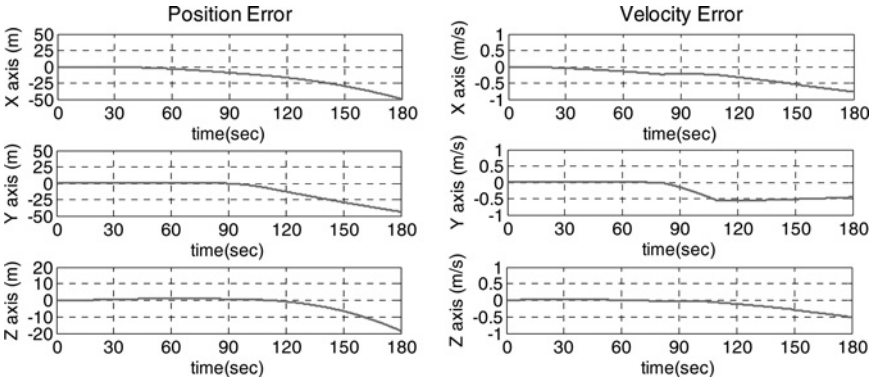

Fig. 6 *Position and velocity errors of INS with the civil grade IMU*

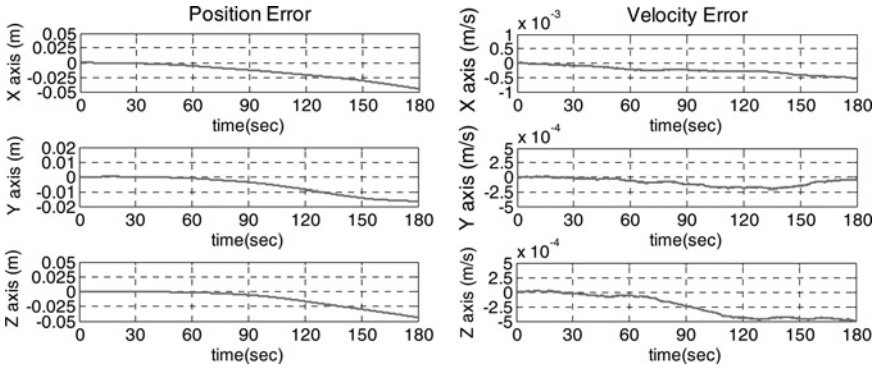

Fig. 7 *Position and velocity errors of INS with the tactical grade IMU*

The presence of the Doppler estimation errors is inevitable since the IMUs used for the INS-aided acquisitions are not free of errors. The acquisition performance would be seriously affected if the Doppler estimation errors exceed the frequency search space. In the experiments, the constellation with 12 visual satellites can be obtained from the received ephemeris in the designed scenario. According to this constellation and the aforementioned IMUs, the Doppler estimation of every satellite can be calculated by (3). Comparing the estimation Doppler with the real Doppler, the Doppler estimation errors of total 12 satellites are computed. The Doppler estimation errors of PRN2 and PRN4 are illustrated in Fig. 8, while the maximum Doppler estimation errors of total satellites are listed in Table 4. From these figures and table, it can be seen that the Doppler estimation errors increase as the quality of IMU decreases. The output error of MEMS IMU1 would seriously reduce the Doppler estimation accuracy and the INS-aided acquisition performance. However, other IMUs can guarantee the INS-aided acquisition performance since

Table 3 Maximum position and velocity errors of the INSs with four different IMUs

Maximum error		MEMS1	MEMS2	Civil grade	Tactical grade
position, m	*x*-axis	10 000	800	50	0.045
	y-axis	14 000	800	42	0.016
	z-axis	8000	500	18	0.04
velocity, m/s	*x*-axis	180	13	0.75	0.0005
	y-axis	180	10	0.55	0.0002
	z-axis	180	11	0.5	0.0005

doi: 10.1049/iet-rsn.2012.0362

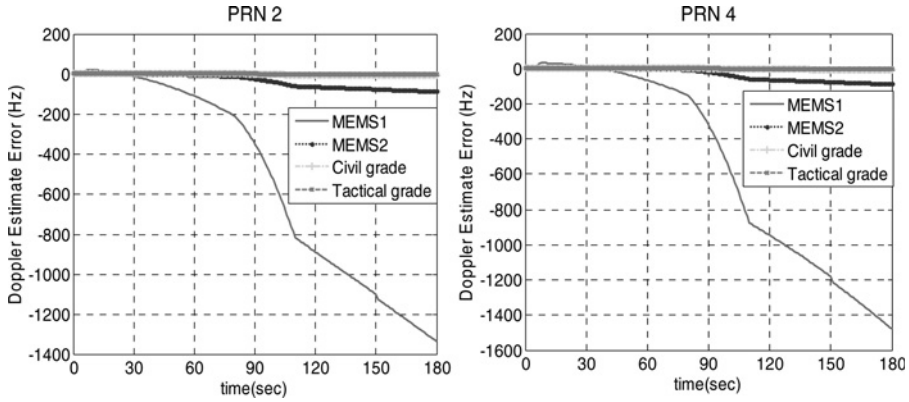

Fig. 8 *Doppler estimation error of PRN2 and PRN4*

Table 4 Maximum Doppler estimation errors of total satellites

	MEMS1, Hz	MEMS2, Hz	Civil grade, Hz	Tactical grade, Hz
PRN2	1336.28	86.81	7.41	3.16
PRN4	1479.51	87.17	4.76	3.14
PRN9	1460.29	103.15	10.02	4.78
PRN10	706.98	43.50	3.68	3.68
PRN13	1240.11	93.44	10.07	5.29
PRN17	914.96	44.17	5.32	5.17
PRN20	107.91	14.35	3.91	2.92
PRN23	1087.03	84.42	11.78	7.41
PRN24	694.71	49.42	6.41	3.67
PRN27	1430.52	101.15	11.22	6.10
PRN28	674.81	46.58	9.74	9.07
PRN32	418.63	32.18	4.72	3.63

their Doppler estimation errors is less than the minimal frequency search space (± 500 Hz) in 180 s. In addition, the Doppler estimation errors significantly increase as long as the accelerometer bias is over 1 mg. This result is in consistent with the analysis in Section 3.

5.4 INS-aided acquisition experiments and results

In the high dynamic scenario, which is described in Section 5.1, the INS-aided acquisition with the four selected IMUs and an unaided acquisition are performed, respectively. The GNSS constellation is built and the satellite radio frequency (RF) signal is transmitted from a HwaCreat™ GNSS signal simulator, which can simulate a real satellite RF signal

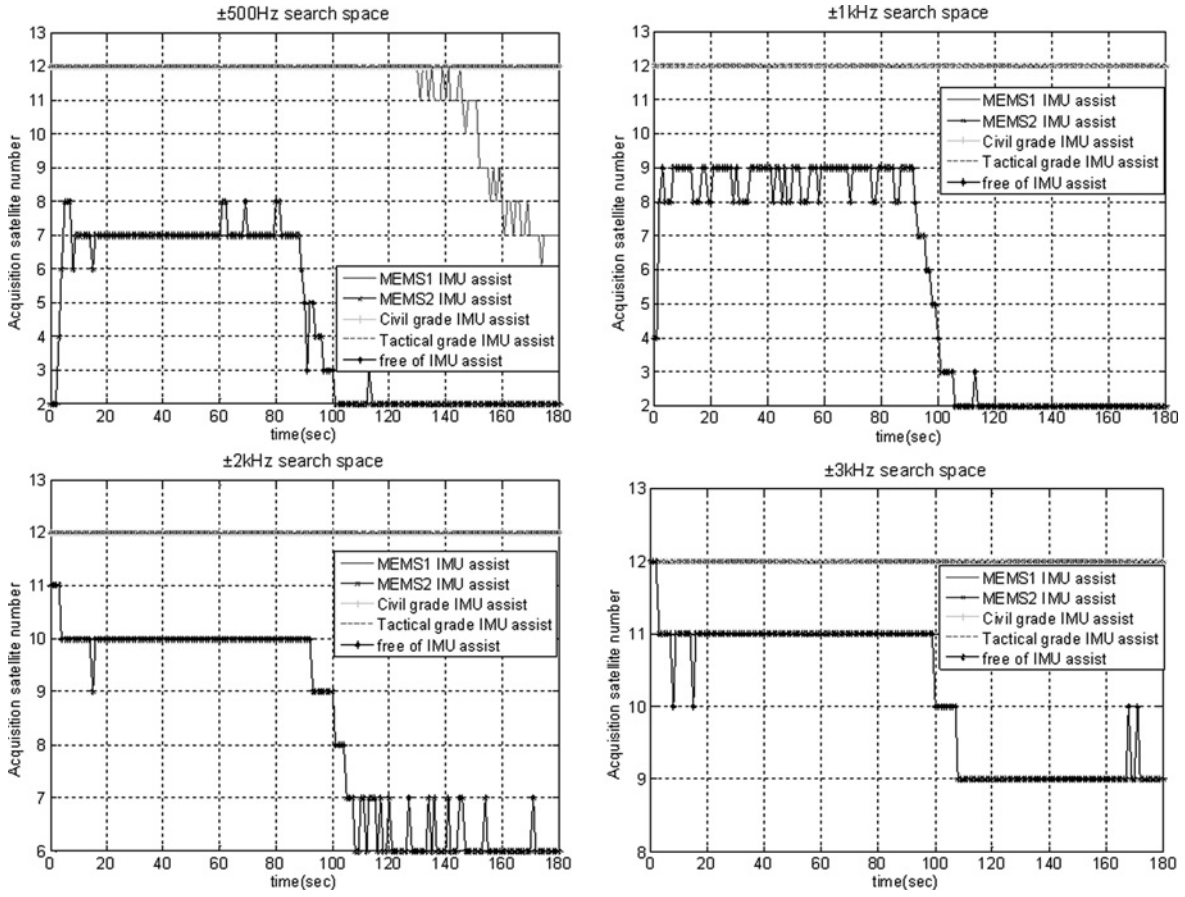

Fig. 9 *Number of the satellites acquired by the receivers with different search spaces*

according to the designed scenario. Then, the RF signal is collected by an RF frontend (MAX 2769) and converted to an intermediate frequency (IF) digital signal for the process of a software receiver. The INS-aided acquisition is the first essential module or component of the software receiver.

Before the INS-aided acquisition experiments, the clock error of the software receiver has been compensated by the method mentioned in Section 2. Hence, the main residual frequency shift is the Doppler shift caused by the relative motion between the satellite and the receiver. In this case, the improvement induced by the INS aid can be fully verified. In Fig. 9, the number of the visual satellites acquired by the INS-aided receivers with different grade IMUs and a standard unaided receiver is illustrated. In the experiments, the frequency search spaces of the local signal are ± 500 Hz, ± 1 kHz, ± 2 kHz and ± 3 kHz, respectively.

From these figures, it is can be seen that the number of the acquired satellites in the INS-aided acquisition is obviously more than that in the unaided acquisition. In Fig. 9, the ± 500 Hz search space cannot guarantee that the total 12 satellites are always acquired by the MEMS IMU1 aided receiver in 180 s due to their large Doppler estimation errors. However, this problem is solved as the search space increases. Meanwhile, from the number change of the acquired satellites in the unaided acquisition, it can be proved that the acquisition capability is stronger when the search space is larger, and the direction change described in Section 3 of the simulation scenario would obviously reduce the number of the acquired satellites. In addition, it can be seen that the velocity change described in Section 1 has an effect on the number of the acquired satellites in Fig. 9.

To summarise the experimental results mentioned above, the INS-aided acquisition has clear advantages compared to the traditional unaided acquisition in the following ways: (1) The local frequency search space and acquisition time are significantly reduced, whereas the number of acquired satellites has increased; (2) Since the experiments are performed in high-dynamic scenario, the application of the INS-aided acquisition on high-speed vehicles is simulated and proved; (3) According to the acquisition result comparison of the INS-aided receivers with different grade IMUs, the MEMS IMU2 is the best choice, which can acquire all satellites with lowest cost and lest search space in 180 s.

6 Conclusions

The INS-aided acquisition scheme based on a parallel code phase search is proposed. It is used to estimate and remove the Doppler shifts contributed by the motions of the satellites and receivers in high dynamics. Then, the error sources of the Doppler estimation are analysed and its relation to the quality of the IMU is derived in detail. To analyse the effect of the IMU quality on the Doppler estimation accuracy and acquisition performances, the acquisitions with different grade IMUs and without IMU are performed in the simulated high-dynamic scenario. The results show that the INS-aided acquisition in high-dynamic applications can reduce the frequency search space and achieve fast acquisition. Moreover, the acquisition comparisons of receivers aided by different grade IMUs shows that the quality of the selected IMU has an effect on the Doppler estimation accuracy and acquisition performance. According to the simulation results, the most suitable IMU is determined in the 180 s simulation scenario.

7 Acknowledgments

This work was supported by a grant from National 863 Programme 'GNSS vulnerability analysis and signal transmission environment (grant no. 2011AA120503)' in China.

8 References

1 Gebre-Egziabher, D.: 'What is the difference between 'loose', 'tight', 'ultra-tight', and 'deep' integration strategies for INS and GNSS?', *Inside GNSS Mag.*, 2007, pp. 28–33
2 Petovello, M.G., Cannon, M.E., Lachapelle, G.: 'Benefits of using a tactical grade INS for high accuracy positioning', *Navigation*, 2004, **51**, (1), pp. 1–12
3 Angrisano, A., Petovello, M., Pugliano, G.: 'Benefits of combined GPS/GLONASS with low-cost MEMS IMUs for vehicular urban navigation', *Sensors*, 2012, **12**, (4), pp. 5134–5158
4 Progri, I.F.: 'An assessment of indoor geolocation systems'. *PhD thesis*, Worcester Polytechnic Institute, Worcester, MA, 2003
5 Alban, S.: 'Design and performance of a robust GPS/INS attitude system for automobile applications'. *PhD thesis*, Stanford University, 2004
6 Ye, P., Zhan, X., Zhang, Y.: 'Micro-electro-mechanical-sensor inertial navigation system-assisted GNSS receiver acquisition scheme and performance evaluation', *J. Shanghai Jiaotong Univ. (Sci.)*, 2011, **16**, (6), pp. 728–733
7 He, X., Hu, X., Tang, K.: 'Analysis of INS aided signal acquisition based on navigation satellites software receivers'. Measuring Technology and Mechatronics Automation, ICMTMA '09, April 2009, pp. 277–280
8 Groves, P.D., Long, D.C.: 'Inertially-aided GPS signal re-acquisition in poor signal to noise environments and tracking maintenance through short signal outages'. ION GNSS 2005, Long Beach, CA, USA, September 2005, pp. 2408–2417
9 Kubrak, D., Monnerat, M., Artaud, G.: 'Improvement of GNSS signal acquisition using low-cost inertial sensors'. ION GNSS 2008, Savannah, GA, USA, September 2008, pp. 2145–2155
10 Kais, M., Millescamps, D., Bétaille, D.: 'A multi-sensor acquisition architecture and real-time reference for sensor and fusion methods benchmarking'. Intelligent Vehicle Symposium 2006, Tokyo, Japan, June 2006, pp. 418–423
11 Garcia, G.: 'A rapid acquisition GPS receiver based on ultra tightly coupled IMU and GPS'. *Master thesis*, Chalmers University of Technology, 2010
12 Angrisano, A., Gaglione, S., Gioia, C.: 'RAIM algorithms for aided GNSS in urban scenario, conference on ubiquitous positioning'. Ubiquitous Positioning, Indoor Navigation, and Location Based Service, Helsinki, Finland, October 2012, pp. 1–9
13 Kubrak, D., Monnerat, M., Artaud, G.: 'Performance analysis of sensor-aided GNSS signal acquisition in signal degraded environments'. ION NTM 2008, San Diego, CA, USA, January 2008, pp. 862–870
14 Parkinson, B., Spilker, J.: 'Global positioning system: theory and applications, Vol. I' (American Institute of Aeronautics and Astronautics, 1996)
15 Borrek, K., Akos, D.M., Bertelsen, N.: 'A software-defined GPS and Galileo receiver: A single-frequency approach' (Birkhäuser, Boston, MA, USA, 2007)
16 Tsui, J.B.: 'Fundamentals of global positioning system receivers a software approach' (Wiley, Hoboken, NJ, USA, 2005, 2nd edn.)
17 Progri, I.F., Bromberg, M.C., Michalson, W.R.: 'The acquisition process of a maximum likelihood GPS receiver'. ION GNSS 2003, Portland, OR, USA, September 2003, pp. 2532–2542
18 Anonymous: 'NAVSTAR GPS space segment/navigation user interfaces', No. ICD-GPS-200C, Department of Defense, 2000
19 Zhang, J., Zhang, K., Grenfell, R.: 'GPS satellite velocity and acceleration determination using the broadcast ephemeris', *J. Navig.*, 2006, **59**, pp. 293–305
20 Savage, P.G.: 'Strapdown inertial navigation integration algorithm design part 2: Velocity and position algorithms', *J. Guid. Control Dyn.*, 1998, **21**, (2), pp. 208–221
21 Ye, P., Du, G., Zhan, X.: 'Performance evaluation of compact MEMS IMU/GPS tight coupling with IMU-aided tracking loop'. ION GNSS 2010, Portland, OR, USA, September 2010, pp. 1636–1644

22 Nassar, S.: 'Improving the inertial navigation system (INS) error model for INS and INS/DGPS applications'. *PhD thesis*, University of Calgary, 2003
23 Flenniken IV, W.S., Wall, J.H., Bevly, D.M.: 'Characterization of various IMU error sources and the effect on navigation performance'. ION GNSS 2005, Long Beach, CA, USA, September 2005, pp. 967–978
24 Qin, F., Zhan, X., Zhang, Y.: 'Simulation of rapid transfer alignment considering body flexure and data delay on dynamic base', *J. Aeronaut. Astronaut. Aviat. Ser. A*, 2011, **43**, (4), pp. 261–268
25 Ohlmeyer, E.J.: 'Analysis of an ultra-tightly coupled GPS/INS system in jamming'. PLANS 2006 IEEE/ION, San Diego, CA, USA, April 2006, pp. 44–53
26 Lashley, M., Bevly, D.M.: 'A comparison of the performance of a non-coherent deeply integrated navigation algorithm and a tightly coupled navigation algorithm'. ION GNSS 2008, Savannah, GA, USA, September 2008, pp. 2123–2129
27 Progri, I.: 'Geolocation of RF signals simulations' (Springer Science & Business Media, New York, NY, USA, 2011)